High Seebeck Coefficient in Mixtures of Conjugated Polymers

Guangzheng Zuo, Xianjie Liu, Mats Fahlman and Martijn Kemerink

Zuo, G., Liu, X., Fahlman, M., Kemerink, M., (2018), High Seebeck Coefficient in Mixtures of Conjugated Polymers, *Advanced Functional Materials*, 28(15), 1703280.
https://doi.org/10.1002/adfm.201703280

WILEY-VCH

DOI: 10.1002/ ((please add manuscript number))
Article type: Full Paper

High Seebeck coefficient in Mixtures of Conjugated Polymers

Guangzheng Zuo, Xianjie Liu, Mats Fahlman and Martijn Kemerink *

G. Zuo, Prof. M. Kemerink
Complex Materials and Devices, Department of Physics, Chemistry and Biology, Linköping University, 58183, Linköping, Sweden
E-mail: martijn.kemerink@liu.se

Dr. X. Liu, Prof. M. Fahlman
Division of Surface Physics and Chemistry, Department of Physics, Chemistry and Biology, Linköping University, 58183 Linköping, Sweden

Keywords: Seebeck coefficient, organic thermoelectrics, conjugated polymers, doping, kinetic Monte Carlo simulations

Abstract

We demonstrate a universal method to obtain record-high electronic Seebeck coefficients while preserving reasonable conductivities in doped blends of organic semiconductors through rational design of the density of states (DOS). A polymer semiconductor with a shallow HOMO level (P3HT) was mixed with materials with a deeper HOMO (PTB7, TQ1) to form binary blends of the type $P3HT_x:B_{1-x}$ ($0 \leq x \leq 1$) that were p-type doped by F_4TCNQ. For B = PTB7, we achieve a Seebeck coefficient $S \sim 1100$ μV/K with conductivity $\sigma \sim 0.3$ S/m at $x = 0.10$, while for B = TQ1 we find $S \sim 2000$ μV/K and $\sigma \sim 0.03$ S/m at $x = 0.05$. Kinetic Monte Carlo simulations with parameters based on experiments show good agreement with our experimental results, confirming the intended mechanism. The simulations are used to derive a design rule for parameter tuning. These results can become relevant for low-power, low-cost applications like (providing power to) autonomous sensors, in which a high Seebeck coefficient translates directly to a proportionally reduced number of legs in the thermogenerator, and hence in reduced fabrication cost and complexity.

1. Introduction

Thermoelectric generators (TEG) can turn temperature differences directly to electricity. Depending on the desired scale of power, there are two different application directions: type I is the large power case, which needs a high figure of merit $ZT = \sigma S^2/\kappa T$ (σ: electrical conductivity, S: Seebeck coefficient, κ: thermal conductivity and T: temperature), to harvest (waste) heat at maximum efficiency. Type II is the low power case in which voltage is more important than power, e.g. to supply an autonomous sensor or a reflective LCD display with electricity. Here, power in the 0.01-1 mW range is sufficient and this type of TEG does not need high ZT, but is sensitive to cost and availability. Low cost implies flexible and easy fabrication, which is not compatible with a large number of legs in the TEG. Hence, a large output voltage $\Delta V = S\Delta T$, with ΔT the temperature difference over the TEG, per leg is needed. In other words, this type of TEG requires a high Seebeck coefficient and a reasonable conductivity. This work focuses on type II TEGs.

Conjugated polymers (CPs) are increasingly explored for thermoelectric applications.[1–3] Compared to inorganic materials, CPs (potentially) offer numerous advantages, such as low cost, large-area deposition, elasticity and flexibility, material abundance and non-toxicity, and an inherently low thermal conductivity. Roughly spoken, CPs for thermoelectric applications can be classified according to the possible relevance for either of these types of TEG: in one limit sit highly (typically oxidatively) doped materials as PEDOT:PSS and its derivatives. These have high conductivity but low Seebeck coefficient, typically well below 100 µV/K. For example, Fan et al. used DMF and $ZnCl_2$ to treat PEDOT:PSS and achieved conductivity over 1×10^5 S/m but only $S \sim 26.1$ µV/K.[4] Bubnova et al. have shown PEDOT:Tos films with $\sigma \sim 10^4$ S/m with $S \sim 200$ µV/K, giving ZT ~ 0.25.[5] These materials could become relevant to Type I applications. In the other limit sit (nearly) intrinsic CPs like P3HT, PBTTT, which have low conductivity but high S, typically around several hundred µV/K. The Seebeck

coefficient of those un-doped CPs is hard to measure directly due to their low conductivity, but it is possible to take a hint from measurement based on OFET devices. For instance, Venkateshvaran et al. indicated that the Seebeck coefficient of PBTTT and IDTBT ranges from 700 to 400 μV/K upon varying the charge density from 10^{18} to 10^{20} cm^{-3} in OFET devices.[6] Zhang et al. achieved S = 480 to 100 μV/K for σ in the range from 10^{-2} to 10 S/m for P3HT and PBTTT.[7] This limit is suitable for neither Type I nor II TEG due to its low conductivity. Evidently, the conductivity of intrinsic CP can be increased by chemical doping. E.g. using $FeCl_3$ or $NOPF_6$ as dopants, the conductivity of P3HT can be improved up to 700–2100 S/m, while sacrificing S that drops to 74–30 μV/K.[8,9]

Alternatively, Zhao et al. have investigated the ionic polymer electrolyte PEO-NaOH that has a very high (ionic) Seebeck coefficient around 7000–10000 μV/K.[10,11] However, this kind of ionic polymer electrolytes do not have DC conductivity, so as to limit their applicability in TEG.

A fundamentally different method to achieve optimized thermoelectric materials was suggested in the seminal work by Mahan and Sofo.[12] They argued that a delta-shaped transport distribution, sitting somewhere above the Fermi level, maximizes the thermoelectric properties. Based on this idea, Sun et al. mixed P3HT with different P3HTT fractions, and, using F_4TCNQ as a p-type dopant, found S increasing from ~580 μV/K for the pristine P3HT to 700 μV/K for P3HT mixed with 2% P3HTT, while maintaining a conductivity around 1.5×10^{-2} S/m.[13]

Here, we revisit the concept proposed by Mahan and Sofo to engineer the charge carrier DOS to maximize thermoelectric performance. In particular, we use the unique possibility offered by molecular semiconductors to make new materials through simple mixing in solution prior to film deposition. We selected conjugated polymers with different HOMO energy levels, P3HT, PTB7 and TQ1, and mixed P3HT with varying fractions of PTB7 and TQ1, respectively. We used (p-type) surface doping by F_4TCNQ to enhance conductivity without

distorting the film morphology.[14] At optimal mixing ratio, the Seebeck coefficient largely exceeds that of either of the pure materials (1100 µV/K at $P3HT_{0.1}$:$PTB7_{0.90}$ and 2000 µV/K at $P3HT_{0.05}$:$TQ1_{0.95}$ vs. 142 µV/K, 469 µV/K and 1560 µV/K for pure P3HT, PTB7 and TQ1, respectively). The observed trends in Seebeck coefficient were in good agreement with kinetic Monto Carlo simulations with parameters based on our experiments.

2. Concept

Charge and energy transport in energetically disordered organic semiconductors as studied here is generally understood to occur through thermally activated tunneling, i.e. hopping.[15] According to percolation theory, the conductivity of such a system is determined by a characteristic hop. Beyond the Boltzmann limit, i.e. at charge concentrations that are relevant to thermoelectric applications, this characteristic hop takes place between the Fermi energy E_F and a so-called transport energy E_{tr}.[16,17] At a given temperature T the Seebeck coefficient S is then simply given by $S = (E_F - E_{tr})/T$. Note that depending on the shape of the DOS and the details of the hopping formalism both E_F and E_{tr} may depend on T.[17,18] Moreover, in this discussion we shall for simplicity assume that the characteristic hop for charge transport is also a relevant measure for the energy transport. In the discussion of our simulation model we shall come back to this.

For pure semiconductor materials, E_F is determined by the charge concentration that, in turn, is determined by the dopant concentration[19,20], see left- and rightmost panels of Figure 1. In case of a Gaussian DOS, E_{tr} is located slightly above the maximum of the DOS. Note that Figure 1 refers to hole transport, hence E_F lays above E_{tr}. When material B, with a deeper HOMO, is mixed into material A, a binary mixture A_x:B_{1-x} with a double-peaked DOS is created. At high and intermediate fractions x both E_F and E_{tr} remain located on the A-part and only a minor increase in S is expected due to the decreased number density in the (part of the) DOS that is explored by the charge carriers: the holes remain entirely on material A, see panel labeled 50% in Figure 1. However, with further increasing B-fraction (decreasing x), E_{tr}

gradually shifts into the B-part of the DOS, reflecting the fact that there are insufficient A-sites to form the optimal percolating network. At the same time, for doping concentrations below 10^{-2}–10^{-1} E_F will remain situated on the A-part of the DOS for any practical loading of material A, i.e. as long as the concentration of material A is significantly larger than the doping concentration. The panel labeled 10% A in Figure 1 reflects the resulting situation. Although the B-part of the DOS is not a delta-function but rather is broadened due to energetic disorder, this situation resembles the original Mahan and Sofo idea of a peaked, delta-shaped transport level sitting relatively far above the Fermi energy. The Seebeck coefficient is expected to peak here, accompanied by a minimum in conductivity. The broadening of especially the B-part of the DOS will suppress the enhancement of *S*, in particular when the energy difference between A and B becomes small. When further increasing the B-fraction, ultimately up to pure B, E_F will also shift to material B, i.e. any remaining fraction of material A becomes a filled trap that does not affect transport. Summarizing, since the Seebeck coefficient is proportional to the gap between E_F and E_{tr}, we can engineer *S* by carefully tuning the mixture of two CPs with different HOMO levels. The maximum attainable value for *S* can be expected to increase with increasing HOMO energy difference, while the composition at which this maximum occurs can be expected to shift to smaller A-fractions as the increasing energetic penalty for hopping to material B will promote hops within material A: for increasing energy difference, charges will ‘try’ to stay longer in the material with the shallow HOMO level. Note that within the framework of this concept, there is no difference between a single material with a doubly peaked DOS and a mixture of distinct materials, each with a singly peaked DOS, irrespective of e.g. the degree of overlap between the two DOS peaks.

3. Results and discussion

To accentuate the generality of the concept introduced above, we selected three well-characterized CPs with different HOMO energies, P3HT, PTB7 and TQ1, and doped these

with the commonly used p-type dopant F_4TCNQ. We used the method proposed by Scholes et al., in which doping is performed by spin coating a dopant-containing solution over an already deposited semiconductor film, preserving the morphology of the latter.[14] Full compound names are given in the experimental section along with further experimental details.

3.1. Energy levels

The ionization potential (IP) and Fermi energy of our CPs were investigated by ultraviolet photoemission spectroscopy (UPS). The UPS spectra are shown in **Figure 2**, the extracted IP and E_F values are tabulated in **Table 1**. From the differences in IP, the energy gap ΔE_{HOMO} between P3HT and PTB7 and between P3HT and TQ1 is around 0.3 eV and 0.5 eV, respectively. Hence, we use P3HT as the shallower-HOMO material A and PTB7 and TQ1 as the deeper-HOMO materials B, c.f. **Figure 1**.

3.2. Seebeck coefficient and conductivity

The conductivity and Seebeck coefficient have measured based on lateral devices in which the active layer is contacted by Ohmic MoO_3/Al contacts. The active layer is the film of P3HT blended with different fractions of PTB7 and TQ1, p-type doped with F_4TCNQ. The results show in **Figure 3**, together with the corresponding power factor $PF = \sigma S^2$.

Focusing on the pure compounds in Figure 3a first, the HOMO level of P3HT is situated closer to the vacuum level than the F_4TCNQ LUMO, which leads to an efficient electron transfer from the HOMO of P3HT to the LUMO of F_4TCNQ.[21] In combination with the used doping procedure, this leads to a high hole density while preserving the morphology of the P3HT, giving a conductivity of pure P3HT of over 400 S/m, which is very comparable with that found in Ref.[14]. The corresponding thermopower is a mere S = 142 µV/K, giving a power factor around 8 µW/K^2·m. PTB7 gives σ = 0.56 S/m and S = 469 µV/K when surface doped by the same procedure as used for P3HT. Since PTB7 has a deeper laying HOMO than P3HT, the lower conductivity and higher thermopower are likely to be due to less efficient electron transfer[19,20], possibly in combination with a minor effect of a larger energetic

disorder in PTB7. Interestingly, when P3HT is blended with different fractions of PTB7, the thermopower reaches a peak value of over 1100 µV/K for 90% PTB7, while the conductivity dropped to a minimum at 0.3 S/m. We attribute this to the mechanism outlined in Figure 1, i.e. the large PTB7 fraction enforces E_{tr} to lay on the PTB7 part of the total DOS, whereas E_F is still located on the P3HT part. The maximum in $\boldsymbol{E_F - E_{tr}}$ translates directly into a maximum in *S*, and, since the characteristic hop requires thermal activation over the same energy difference, in a minimum in the conductivity.

TQ1 has a deeper laying HOMO than both PTB7 and P3HT, leading, for the same doping procedure with F_4TCNQ, to a low conductivity of 0.03 S/m and a surprisingly high thermopower around 1560 µV/K, again attributed to difficulty of electron transfer between TQ1and F_4TCNQ and possibly a higher disorder in the amorphous TQ1 than in the semi-crystalline P3HT [20]. On basis of the mechanism outlined in Figure 1, it is to be expected that any peak in binary blends of P3HT with TQ1 should (a) be higher than that of P3HT:PTB7 and (b) should occur at even higher loadings of the B-component, i.e. beyond 90% TQ1. Indeed, in Figure 3b we find that the Seebeck coefficient increases steeply up to ~2000 µV/K at 95% TQ1, which is both higher than P3HT:PTB7 and pure TQ1.

To highlight the fact that the peaked shape of the *S* vs. composition curves is not a straightforward blending effect, the dashed lines in Figure 3 show the interpolation between the binary extremes using an effective medium model. In that case, *S* of the blend would be the linear combination of the Seebeck coefficients of the constituents weighted by their electrical conductivities, viz. $S(x) = (x\sigma_A S_A + (1-x)\sigma_B S_B)/(x\sigma_A + (1-x)\sigma_B)$ with *x* the fraction of material B and $\sigma_{A/B}$ and $S_{A/B}$ the values of the pure compounds. Clearly, the effective medium scheme fails to reproduce the peak in *S*, and the concomitant dip in conductivity, indicating that electronic interactions, in this case by hopping between A and B sites, are responsible for the observed behavior.

Putting our results in perspective, the characteristic numbers reported here (S = 1100 µV/K, σ = 0.3 S/m and PF = 0.3 µW/K^2·m for P3HT:PTB7 (90%) and S = 2000 µV/K, σ = 0.03 S/m and PF = 0.1 µW/K^2·m for P3HT:TQ1 (95%)) are all significantly higher than the values reported for the P3HT:P3HTT system in the pioneering work by Sun et al.[13], where S ~ 700 µV/K, σ ~ 0.015 S/m and PF ~ 7×10^{-3} µW/K^2·m were reported.

3.3. kinetic Monto Carlo simulations

To put a more formal basis to the findings above, and in particular to establish that indeed the mechanism of Figure 1 is the dominant factor determining the thermopower maxima found in Figure 3, we performed numerical kinetic Monte Carlo simulations. The employed model has been described in detail before [19,20,22] and treats the charge and energy transport as nearest neighbor hopping, quantified by Miller-Abraham rates, on a cubic lattice with site energies drawn from a Gaussian distribution. Importantly, all Coulomb interactions, i.e. hole-hole and hole-ion, are explicitly accounted for. The used input parameters come, where possible, from experiment and are given in the caption of **Figure 4**. Although the employed surface doping procedure gives reproducible results in terms of σ and S, with typically ~10% sample-to-sample variation, it is not straightforward to determine the exact F_4TCNQ concentration in the film after the doping step. Therefore, we ran the simulations with doping concentrations from 10^{-3} to 10^{-1}. We considered A_x:B_{1-x} mixtures, using differences in HOMO energies between the A and B compounds of 0.3 eV (Figure 4a-c), corresponding to the P3HT:PTB7 case, and 0.5 eV (Figure 4d-f), corresponding to the P3HT:TQ1 case. To make the results as transparent as possible, all other parameters like the energetic disorder were kept constant for all materials and their combinations. Sites corresponding to materials A and B where taken to be randomly distributed according to the desired ratio x.

In the simulations, the Seebeck coefficient is calculated as

$$S = \int_{-\infty}^{\infty} dE \frac{(E - E_F)\sigma(E)}{\sigma T}$$

where the conductivity σ is related to the conductivity distribution function $\sigma(E)$ through $\sigma = \int_{-\infty}^{\infty} dE\sigma(E)$. [23] Hence, defining an 'energy-transport energy' as

$$E_{E,tr} = \int_{-\infty}^{\infty} dE \frac{E\sigma(E)}{\sigma T}$$

one recovers the expression $S = \left(E_F - E_{E,tr}\right)/T$ used in section 2 above. Although a full discussion of the relation between E_{tr} and $E_{E,tr}$ is beyond the scope of the present paper, we notice that using E_{tr}, as calculated from the analytical percolation model in Ref. [19] instead of $E_{E,tr}$ gives a relatively minor overestimation of *S*: for a single compound with material parameters as used in this work, the difference is a constant ~100 µV/K over the full concentration range of 10^{-5} – 10^{-1} over which *S* varies between ~1100 – ~100 µV/K as shown in the Supporting Information. The offset reflects the fact that not all (energetically upward) hops are to the critical energy that determines the conductivity of the percolating network, i.e. $E_{E,tr}$ lies below E_{tr}.

For both Figures 4a-c and 4d-f, we find that the simulated conductivity decreases with increasing B fraction, and that the trend is similar in both shape and span to what we found in our experimental results as shown in Figure 3. The sudden drop in conductivity in going from pure P3HT to a 10% blend, c. f. Figure 3, is however absent from the model. We speculate it is caused by a disruption of the crystalline morphology of P3HT upon mixing with another conjugated material. As in the simulations compounds A and B and their mixtures are assumed to have the same disorder, this corroborates that the main reason for the lower conductivity (and higher Seebeck coefficient) in pure PTB7 and TQ1, as compared to P3HT, is their unfavorable HOMO energy with respect to the LUMO of F_4TCNQ that leads to a lower mobile charge concentration and a larger gap between E_F and $E_{E,tr}$.[20] Note that the magnitude of the simulated conductivity is less important here as it is (trivially) proportional to the largely unknown attempt frequency ν_0. For the Seebeck coefficient such a scaling

parameter does not exist and the calculated numbers truly reflect the energetics in the (idealized) numerical experiment. For all doping concentrations, a peak in *S* between 80% and 100% of part B is found in Figure 4, which is good agreement with our experimental observations. Moreover, for given doping concentration, the peak is higher and sits further to the right for the largest HOMO level offset (panels d-f), again in agreement with experiment. In line with previous analytical calculations, the Seebeck coefficient decreases with increasing doping concentration from 10^{-3} to 10^{-1}, reflecting the shift of E_F towards the E_{tr}, c.f. Figure 1. We also note that with the same doping concentration but different HOMO level offsets, the Seebeck coefficient is almost identical as long as the fraction B is under 60%, since both E_F and E_{tr} are then dominated by the A fraction in the mixture. Comparison of especially the Seebeck coefficient with experiments allows a rough estimate of the actual doping concentration around 10^{-2}. For a total number density of ~10^{27} m^{-3} this corresponds to ~10^{25} m^{-3}, which seems quite reasonable.[14] A more quantitative investigation between doping concentration and Seebeck coefficient is beyond the scope of the present paper and topic of ongoing work. The same holds, mutatis mutandis, for the relation between thermopower and morphology. While the quasi-quantitative agreement between simulations and experiments suggests that energetics are more important than morphology in determining a material's thermoelectric properties, the energetics may of course depend on morphology. Also this is topic of ongoing work.

Having established that our kinetic Monte Carlo simulations capture the key physics governing the thermoelectric properties of doped blends, we shall, in this last section, use these simulations to study the possibilities of generic A:B blends with varying energetics. **Figure 5** shows the calculated peak value of *S* (panel a) and the corresponding conductivities and power factors (panels b, c, respectively) vs. the HOMO energy difference between materials A and B and the dopant LUMO energy w.r.t. the HOMO of material A. Closed symbols indicate the P3HT:PTB7 and P3HT:TQ1 blends considered above. An important

conclusion to be drawn from these simulations is that electronic Seebeck coefficients up to and above 5000 µV/K seem within reach using the design rule outlined above. Unfortunately, there is a clear trade off with the corresponding conductivity that leads to a significant drop in power factor in the regions where *S* reaches more extreme values. In fact, in our simulations the maximum in PF for a given dopant LUMO energy is always found for the pure compound that is easiest doped, i.e. material A. The SI shows the corresponding cross sections for $HOMO_A$-$HOMO_B$ = 0 on linear scale.

Another important feature in Figure 5a is the strong suppression of the peak *S* value with increasing $HOMO_A$-$LUMO_{dopant}$, i.e. when the dopant becomes an efficient dopant for material B too. This remarkable behavior can be understood from the resulting increase in free charge density when not only the minority component A but also the majority component B has a HOMO energy that is in the vicinity of, or even above the dopant LUMO. However, one must also account for the fact that the (increasing) ionization of the dopant leads to a modification of the DOS in the form of the formation of exponential tails that sit below the peaks of the original double Gaussian DOS as shown in the SI.[19] In the numerical model these Coulomb interactions are accounted for and give rise to a Fermi energy that shifts down towards the transport energy that slightly shifts up, explaining the dropping peak value of the Seebeck coefficient with dopant LUMO energy, as shown in Figure 5d.

4. Conclusions

We investigated the thermopower and the conductivity of P3HT blended with PTB7 and TQ1 covering the full range of 0 to 100%. These materials were chosen for their differences in ionization potential (IP = 4.7eV, 5.03eV and 5.16 eV for P3HT, PTB7 and TQ1, respectively, as characterized by UPS), which allows a rational optimization of the Seebeck coefficient through design of the density of states. For $P3HT_{0.10}$:$PTB7_{0.90}$ and $P3HT_{0.05}$:$TQ1_{0.95}$, the Seebeck coefficient peaked at ~1100 µV/K and ~2000 µV/K, respectively, approaching values that so far are only found in ionic thermoelectrics where they are accompanied by an

essentially zero DC conductivity. For the present systems, the conductivity is limited by the poor doping efficiency of the used p-type dopant, F_4TCNQ, in combination with PTB7 and TQ1, suggesting a pathway to further improvement. Furthermore, the results of numerical simulations using a kinetic Monte Carlo model are in good agreement with the experimental data, further confirming the viability and are used to develop a design rule that can guide material optimization in new thermoelectric systems.

5. Experimental Section

Materials: Regioregular-poly(3-hexylthiophene-2,5-diyl) (rr-P3HT), and Poly({4,8-bis[(2-ethylhexyl) oxy] benzo[1,2-b:4,5-b'] dithiophene-2,6-diyl} {3-fluoro-2-[(2-ethylhexyl) carbonyl] thieno[3,4-b] thiophenediyl}) (PTB7) were purchased from 1-Material Inc. Poly [2,3-bis(3-octyloxyphenyl)-5,8-quinoxalinediyl]-2,5-thiophenediyl] (TQ1) was synthesized at Chalmers University of Technology. 2,3,5,6-Tetrafluoro-7,7,8,8-tetracyanoquinodimethane (F_4TCNQ) was purchased from Ossila. All materials were used as received.

Device fabrication: P3HT, PTB7, and TQ1 were dissolved in ortho-dichlorobenzene (o-DCB), respectively, to make solutions of 25 mg/ml. F_4TCNQ was dissolved in a mixture of tetrahydrofuran (THF) and dichloromethane (DCM) in a 4:1 ratio and a concentration of 5 mg/ml. P3HT and PTB7 (or TQ1) were taken by volume to form mixtures with a PTB7 (or TQ1) fraction from 0% to 100%, typically in 10% intervals. The active layers were spin-coated (1000 rpm for 60 seconds and then 3000 rpm for 20 seconds) on top of cleaned glass substrates to get thin films with a thickness around 150 nm as measured with a Dektak surface profilometer. The films were doped by spin-coating F_4TCNQ on the top of active layer at 3000 rpm for 40 seconds. After that MoO_3 (9 nm) and Al (90 nm) were thermally evaporated through a shadow mask under a pressure of 1×10^{-6} mbar to form Ohmic contacts. The contact dimensions are 2 × 7 mm (width × length), defining a 7 × 0.5 mm channel.

Conductivity and Seebeck coefficient measurement: Room temperature electrical characterizations were performed in a glove box under Nitrogen atmosphere. Current voltage

characteristics were obtained between -50mV and 50mV. Conductivities were calculated according to $\sigma = j/F$, where j and F are the current density and electric field, respectively. The thermopower was obtained by applying a linear temperature gradient of various magnitudes along the sample and recording the shift of the *jV*-characteristics at the end of a settling time of ca. 400 seconds. From the change of the thermovoltage ΔV as a function of the temperature difference ΔT between the contacts, the thermopower S was calculated as $S = \Delta V/\Delta T$. All electrical measurements have been done in a Kelvin-probe (4-probe) setup.

UPS measurement: Ultraviolet photoemission spectroscopy (UPS) experiments were carried out using a Scienta ESCA 200 spectrometer in ultrahigh vacuum (1×10^{-10} mbar) with a standard He-discharge lamp with HeI 21.22 eV. The total energy resolution of the UPS measurement is about 80 meV as extracted from the width of the Fermi level of clean gold foil. All spectra were collected at a photoelectron takeoff angle of 0° (normal emission). The work functions of the films were extracted from the determination of the high binding-energy cutoff of the UPS spectra by applying a bias of -3 V to the sample.

Supporting Information

Supporting Information is available from the Wiley Online Library or from the author.

Acknowledgements

The research by G.Z. is supported by the Chinese Scholarship Council (CSC). We are grateful to Hassan Abdallah for technical assistance with the thermoelectric measurements, and Olle Inganäs for the use of technical infrastructure for device fabrication.

References

[1] Y. Xuan, X. Liu, S. Desbief, P. Leclère, M. Fahlman, R. Lazzaroni, M. Berggren, J. Cornil, D. Emin, X. Crispin, *Phys. Rev. B* **2010**, *82*, 115454.

[2] Q. Zhang, Y. Sun, W. Xu, D. Zhu, *Adv. Mater.* **2014**, n/a.
[3] O. Bubnova, X. Crispin, *Energy Environ. Sci.* **2012**, *5*, 9345.
[4] Z. Fan, D. Du, Z. Yu, P. Li, Y. Xia, J. Ouyang, *ACS Appl. Mater. Interfaces* **2016**, *8*, 23204.
[5] O. Bubnova, Z. U. Khan, A. Malti, S. Braun, M. Fahlman, M. Berggren, X. Crispin, *Nat. Mater.* **2011**, *10*, 429.
[6] D. Venkateshvaran, M. Nikolka, A. Sadhanala, V. Lemaur, M. Zelazny, M. Kepa, M. Hurhangee, A. J. Kronemeijer, V. Pecunia, I. Nasrallah, I. Romanov, K. Broch, I. McCulloch, D. Emin, Y. Olivier, J. Cornil, D. Beljonne, H. Sirringhaus, *Nature* **2014**, *515*, 384.
[7] F. Zhang, Y. Zang, D. Huang, C. Di, X. Gao, H. Sirringhaus, D. Zhu, *Adv. Funct. Mater.* **2015**, *25*, 3004.
[8] S. Qu, Q. Yao, L. Wang, Z. Chen, K. Xu, H. Zeng, W. Shi, T. Zhang, C. Uher, L. Chen, *NPG Asia Mater.* **2016**, *8*, e292.
[9] Y. Xuan, X. Liu, S. Desbief, P. Leclère, M. Fahlman, R. Lazzaroni, M. Berggren, J. Cornil, D. Emin, X. Crispin, *Phys. Rev. B* **2010**, *82*, 115454.
[10] D. Zhao, H. Wang, Z. U. Khan, J. C. Chen, R. Gabrielsson, M. P. Jonsson, M. Berggren, X. Crispin, *Energy Env. Sci* **2016**, *9*, 1450.
[11] D. Zhao, S. Fabiano, M. Berggren, X. Crispin, *Nat. Commun.* **2017**, *8*, ncomms14214.
[12] G. D. Mahan, J. O. Sofo, *Proc. Natl. Acad. Sci.* **1996**, *93*, 7436.
[13] J. Sun, M.-L. Yeh, B. J. Jung, B. Zhang, J. Feser, A. Majumdar, H. E. Katz, *Macromolecules* **2010**, *43*, 2897.
[14] D. T. Scholes, S. A. Hawks, P. Y. Yee, H. Wu, J. R. Lindemuth, S. H. Tolbert, B. J. Schwartz, *J. Phys. Chem. Lett.* **2015**, *6*, 4786.
[15] H. Bässler, *Phys. Status Solidi B* **1993**, *175*, 15.
[16] R. Coehoorn, W. F. Pasveer, P. A. Bobbert, M. A. J. Michels, *Phys. Rev. B* **2005**, *72*, 155206.
[17] J. Cottaar, L. J. A. Koster, R. Coehoorn, P. A. Bobbert, *Phys. Rev. Lett.* **2011**, *107*, 136601.
[18] S. D. Baranovskii, *Phys. Status Solidi B* **2014**, *251*, 487.
[19] G. Zuo, H. Abdalla, M. Kemerink, *Phys. Rev. B* **2016**, *93*, 235203.
[20] G. Zuo, Z. Li, O. Andersson, H. Abdalla, E. Wang, M. Kemerink, *J. Phys. Chem. C* **2017**, *121*, 7767.
[21] Q. Bao, X. Liu, S. Braun, F. Gao, M. Fahlman, *Adv. Mater. Interfaces* **2015**, *2*, n/a.
[22] A. Melianas, F. Etzold, T. J. Savenije, F. Laquai, O. Inganäs, M. Kemerink, *Nat. Commun.* **2015**, *6*, ncomms9778.
[23] H. Fritzsche, *Solid State Commun.* **1971**, *9*, 1813.

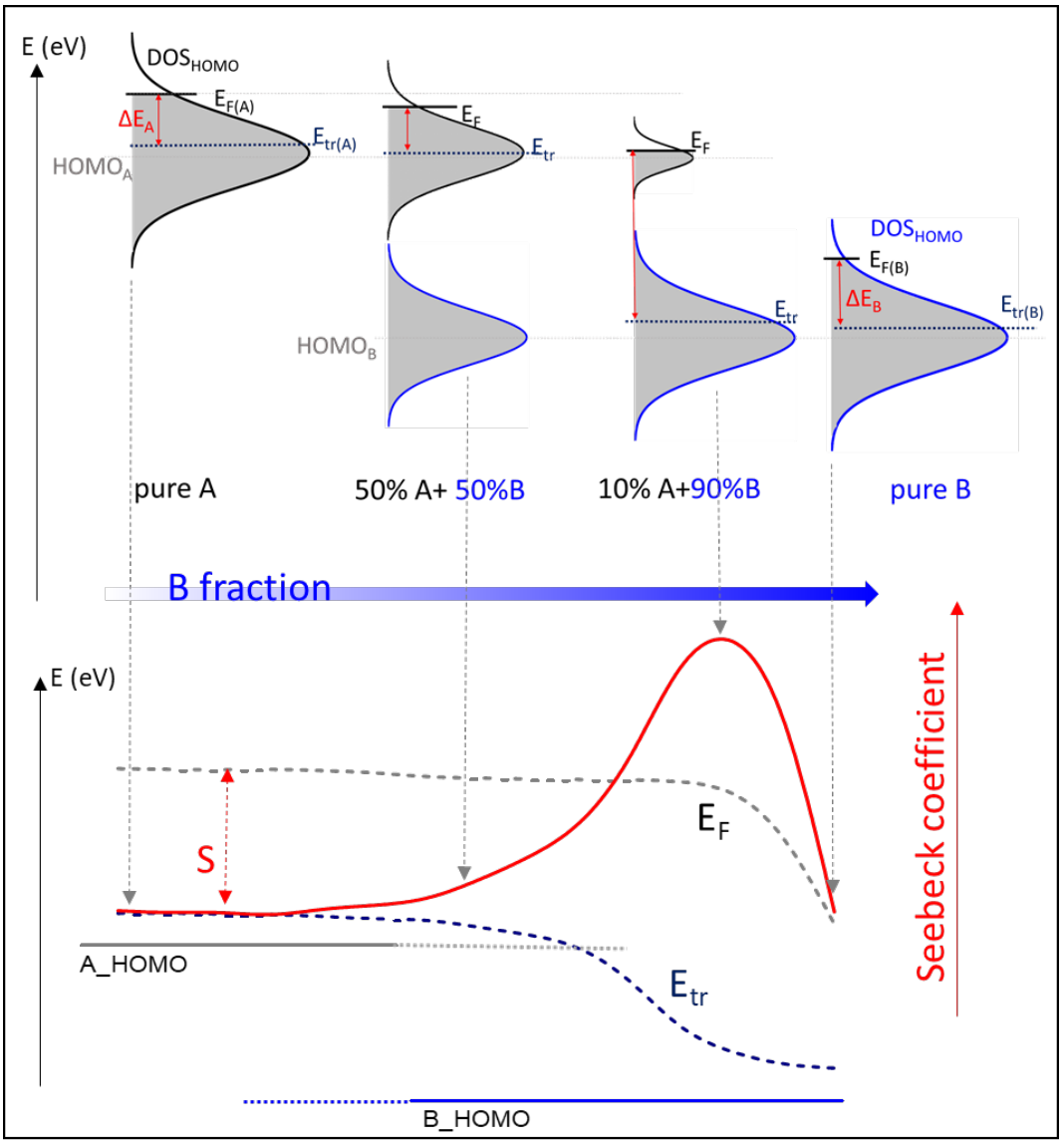

Figure 1 Illustration of DOS engineering to achieve a high Seebeck coefficient. Upper part: hole density of states for a binary mixture A:B. White and shaded regions indicate electron- and hole-filled parts of the DOS, respectively. Lower part: corresponding relative positions of the Fermi energy E_F and the transport energy E_{tr} and the Seebeck coefficient S that is proportional to their difference. See main text for further explanation.

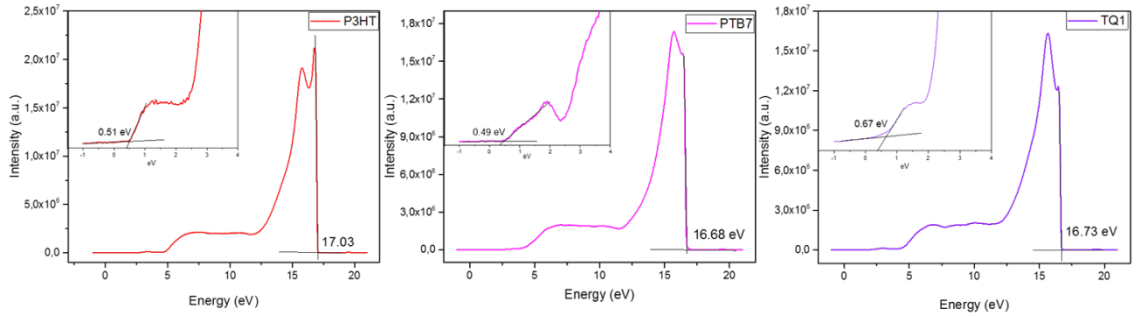

Figure 2 UPS spectra of pristine P3HT, PTB7 and TQ1. Insets show zoom-ins on the frontier valence region. The positions of the secondary electron cut-off and valence band edge are given, from which the IP and E_F (work function) are derived.

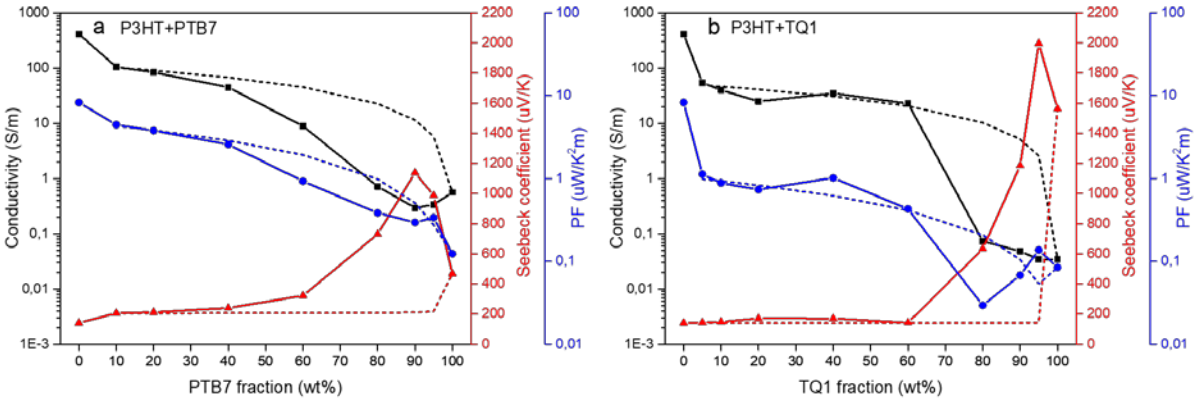

Figure 3 Conductivity, Seebeck coefficient and power factor (PF) for a) P3HT:PTB7; b) P3HT:TQ1, dependent on active layer composition. The dashed lines show the interpolation between the binary extremes using an effective medium model, disregarding the drop at 0 wt%.

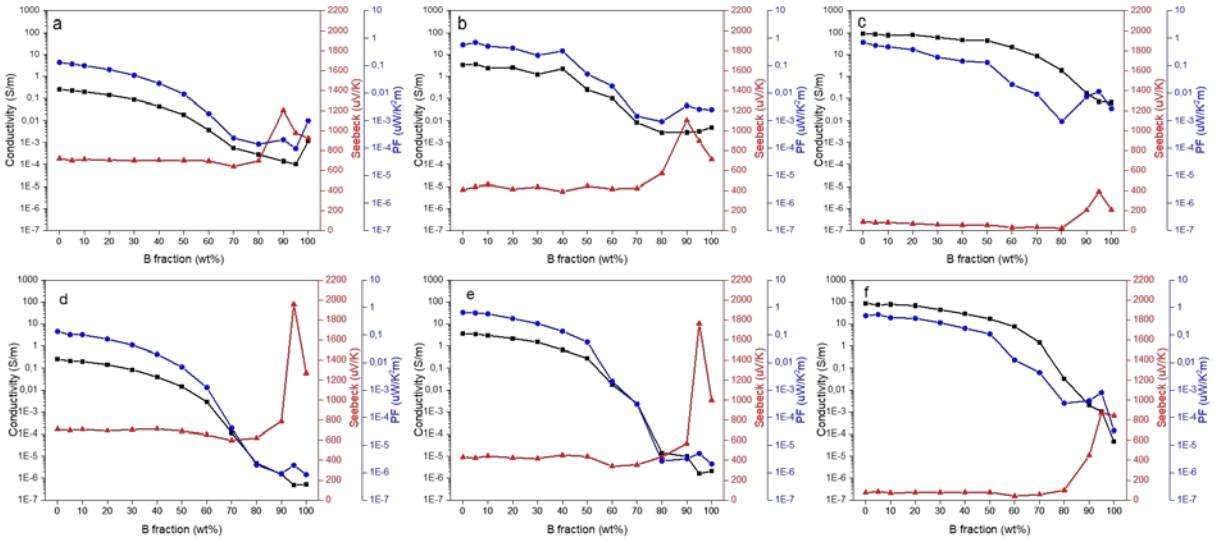

Figure 4 Conductivity, Seebeck coefficient and power factor vs. composition from kinetic Monto Carlo simulations for A_x:B_{1-x} mixtures with HOMO energy differences of 0.3 eV (a-c) and 0.5 eV (d-f) and with doping concentrations of 10^{-3} (a,d), 10^{-2} (b,e) and 10^{-1} (c,f). Parameters used are the attempt to hop frequency $\nu_0 = 10^{-13}$ s^{-1}; intersite distance a_{NN} = 1.8 nm; Gaussian disorder σ_{DOS} = 0.075 eV; temperature T = 300 K; $HOMO_A$ - $LUMO_{dopant}$ = 0.24 eV.

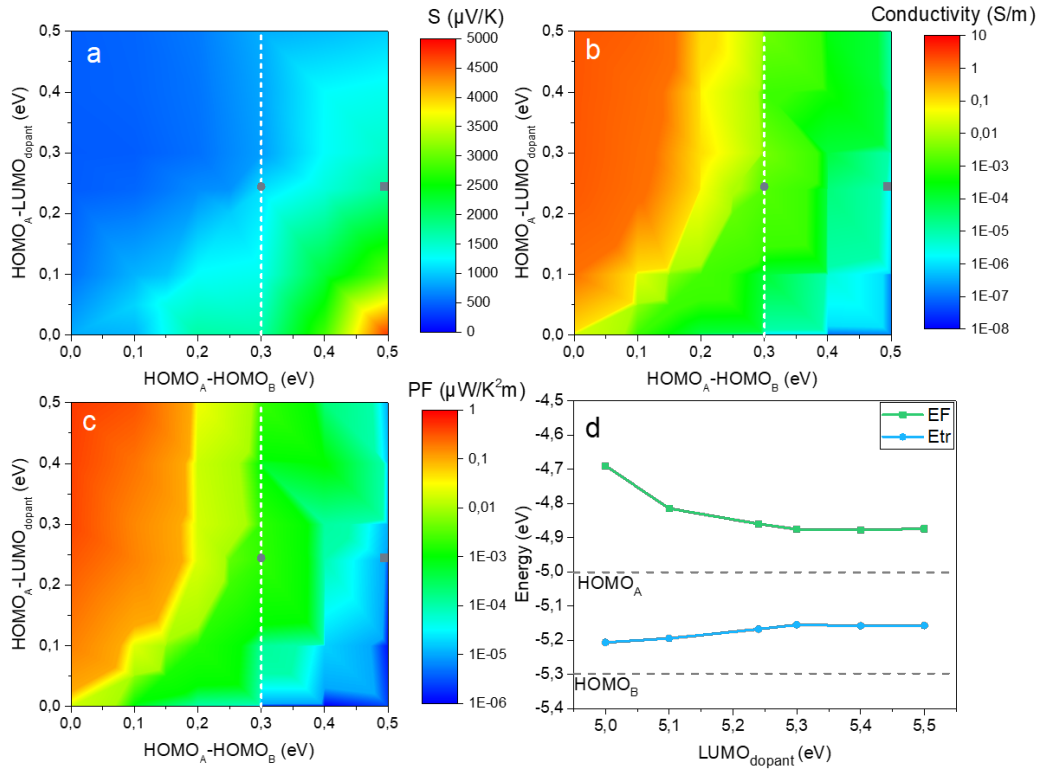

Figure 5 Simulated maximum Seebeck coefficient at peak position dependent on the position of the involved energy levels (a); corresponding conductivity (b) and power factor (c). Closed symbols correspond to the P3HT:PTB7 (circles) and P3HT:TQ1 blends (squares). (d) Fermi energy and transport energy $E_{E,tr}$ vs. dopant LUMO for $HOMO_A - HOMO_B = 0.3$ eV, i.e. along the dashed line in panels a-c. Same parameters as in Figure 4.

Table 1 E_F and IP of the three CPs used in this study deposited onto ITO substrates

CPs	E_F (eV)	IP (eV)
P3HT	4.19	4.7
PTB7	4.54	5.03
TQ1	4.49	5.16

The table of contents entry should be 50–60 words long, and the first phrase should be bold. The entry should be written in the present tense and impersonal style. The text should be different from the abstract text.

Record-high Seebeck coefficients are achieved for p-type doped blends of common conjugated polymers. The method used is based on a rational design of the density of states, such that the characteristic hop occurs from the compound with the shallower HOMO to the compound with the deeper HOMO.

Keyword: Seebeck coefficient, organic thermoelectrics, conjugated polymers, doping, kinetic Monto Carlo simulations

Guangzheng Zuo, Xianjie Liu, Mats Fahlman and Martijn Kemerink *

High Seebeck coefficient in Mixtures of Conjugated Polymers

ToC figure ((Please choose one size: 55 mm broad × 50 mm high **or** 110 mm broad × 20 mm high. Please do not use any other dimensions))

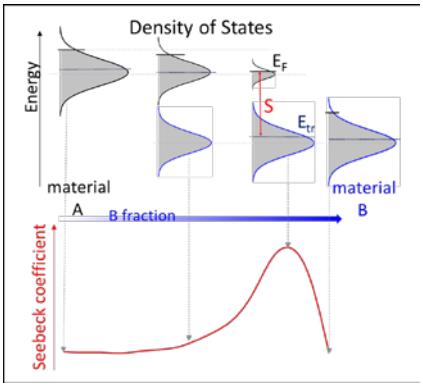

Supporting Information

High Seebeck coefficient in Mixtures of Conjugated Polymers

Guangzheng Zuo, Xianjie Liu, Mats Fahlman and Martijn Kemerink *

Contents

Comparison of Monte Carlo and analytical models

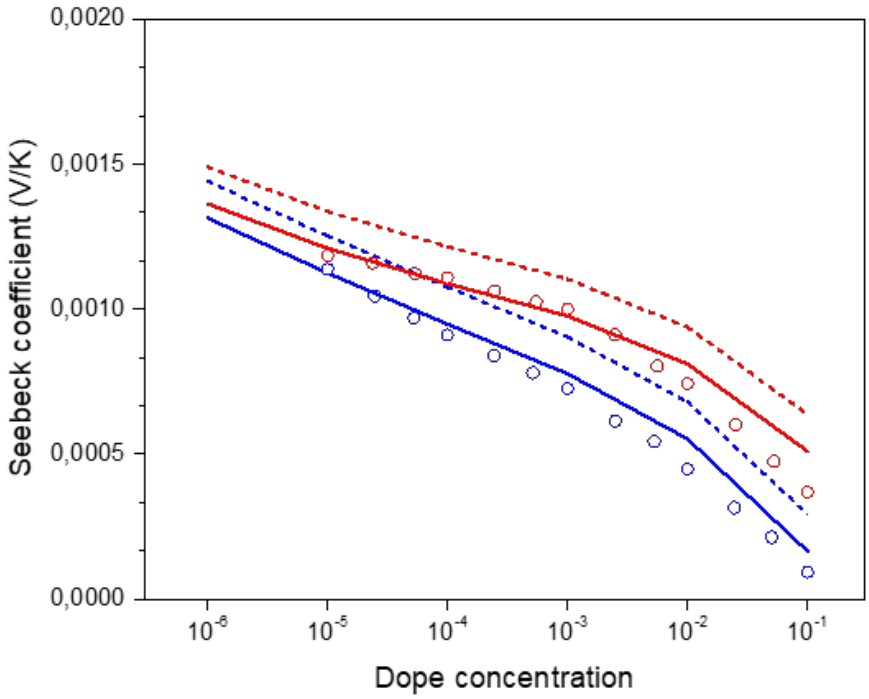

Figure S1 Seebeck coefficient from the analytical model (lines) vs. kinetic Monto Carlo simulations (dots) with different doping concentrations. Parameters used are the attempt to hop frequency ν_0 = 10^{-11} s^{-1}; intersite distance a_{NN} = 1.8 nm; Gaussian disorder σ_{DOS} = 0.075 eV; temperature T = 300 K; HOMO = -5.2 eV; $LUMO_{dopant}$ = -5.2 eV (ΔE= HOMO − $LUMO_{dopant}$ = 0, red) and -5.5 eV (ΔE=0.3, blue); α = 0.491(dashed line) and α = 1 (solid line).

The analytical model is described in Ref. [1]. The Seebeck coefficient is then approximated by $S = (E_F - E_{tr})/T$, with E_{tr} the transport energy defined as the final energy of the conduction-limiting hop from the Fermi energy E_F. The transport energy is assumed to sit slightly below the maximum in the density of states (centered at zero energy) as $E_{tr} = -\alpha\sigma$ with σ the width of the DOS.[2] According to Ref. [2] α = 0.491 for nearest neighbor hopping on a simple cubic lattice as used in the kinetic Monte Carlo model. We found that α = 1 best matches the two models when focusing solely on the Seebeck coefficient, corresponding to an offset in S of ~100 µV/K as mentioned in the main text.

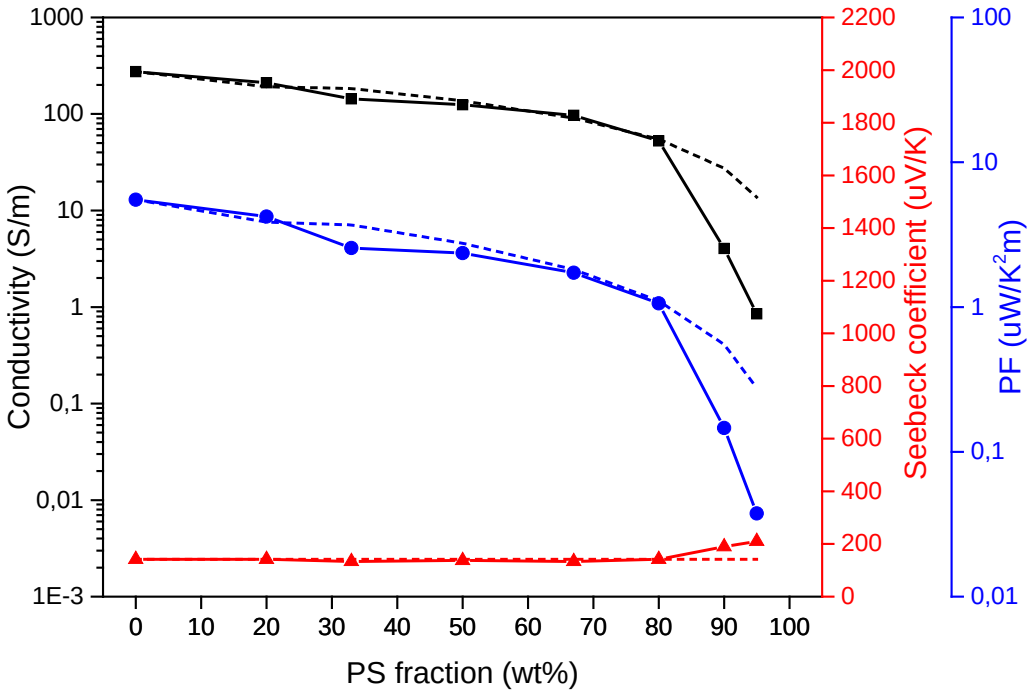

Figure S2 Seebeck coefficient and conductivity of a doped blend of P3HT and polystyrene. The dashed lines show the interpolation between the binary extremes using an effective medium model.

The absence of any peaks in *S* and the good agreement with the effective medium fits in Figure S2 show that the peaks in *S* in the main text are not related to simple dilution effects as e.g. discussed in Ref. [3]. The steep drop beyond 80 wt% is attributed to percolation effects, in particular the formation of isolated P3HT clusters.

Representative densities of states

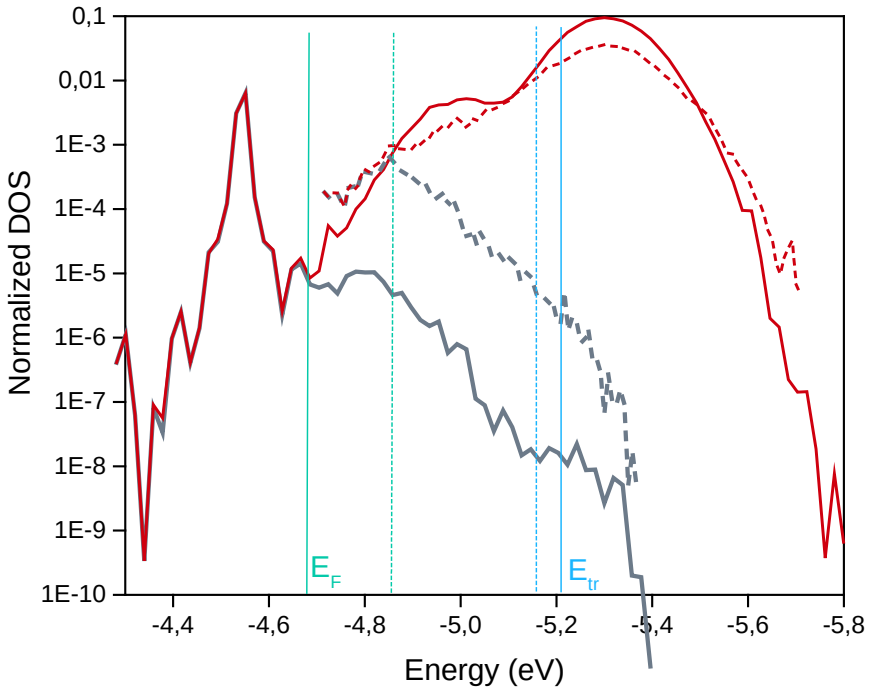

Figure S3 Calculated density of states (red lines) and density of occupied states (dark grey lines) for $HOMO_A$ = -5.0 eV, $HOMO_B$ = -5.3 eV and $LUMO_{dopant}$ = -5.0 eV (solid lines) and $LUMO_{dopant}$ = -5.5 eV (dashed lines). Note the higher Fermi level and stronger broadening of the DOS in the case of the stronger dopant.

Seebeck coefficient, conductivity and power factor for a single material

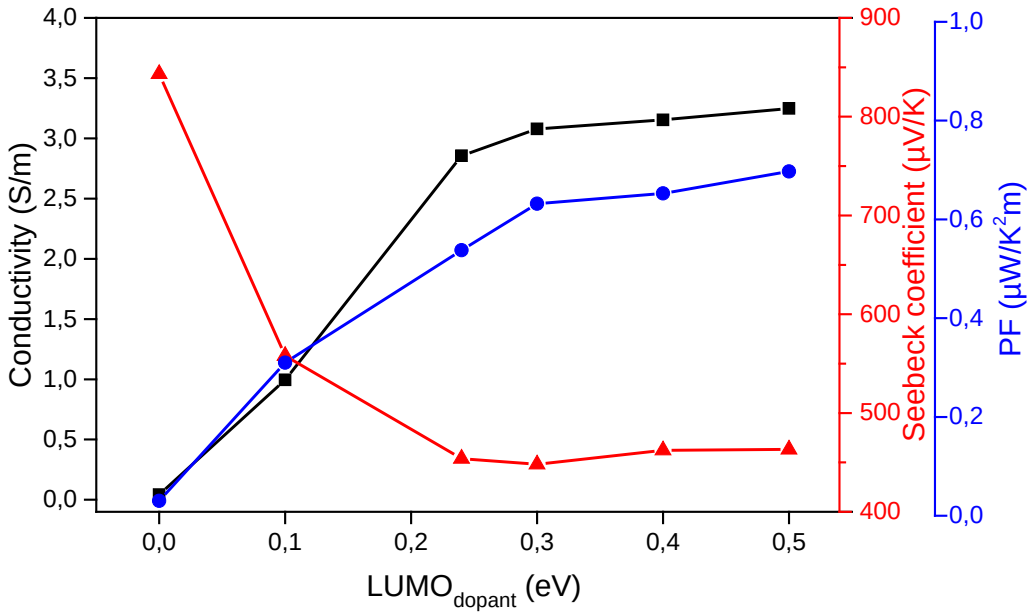

Figure S4 Calculated Seebeck coefficient, conductivity and power factor for a single material, corresponding to $HOMO_A$-$HOMO_B$ = 0 in Figure 5 of the main text.

References

[1] G. Zuo, H. Abdalla, M. Kemerink, *Phys. Rev. B* **2016**, *93*, 235203.
[2] J. Cottaar, L. J. A. Koster, R. Coehoorn, P. A. Bobbert, *Phys. Rev. Lett.* **2011**, *107*, 136601.
[3] D. Abbaszadeh, A. Kunz, G. A. H. Wetzelaer, J. J. Michels, N. I. Crăciun, K. Koynov, I. Lieberwirth, P. W. M. Blom, *Nat. Mater.* **2016**, *15*, 628.